Distinct forms of the actin cross-linking protein α-actinin support macropinosome internalization and trafficking

Kevin M. Burton[a], Katherine M. Johnson[a], Eugene W. Krueger[a], Gina L. Razidlo[a,b,*], and Mark A. McNiven[a,b,*]

[a]Division of Gastroenterology & Hepatology and [b]Department of Biochemistry & Molecular Biology, Mayo Clinic, Rochester, MN 55905

ABSTRACT The α-actinin family of actin cross-linking proteins have been implicated in driving tumor cell metastasis through regulation of the actin cytoskeleton; however, there has been little investigation into whether these proteins can influence tumor cell growth. We demonstrate that α-actinin 1 and 4 are essential for nutrient uptake through the process of macropinocytosis in pancreatic ductal adenocarcinoma (PDAC) cells, and inhibition of these proteins decreases tumor cell survival in the presence of extracellular protein. The α-actinin proteins play essential roles throughout the macropinocytic process, where α-actinin 4 stabilizes the actin cytoskeleton on the plasma membrane to drive membrane ruffling and macropinosome internalization and α-actinin 1 localizes to actin tails on macropinosomes to facilitate trafficking to the lysosome for degradation. In addition to tumor cell growth, we also observe that the α-actinin proteins can influence uptake of chemotherapeutics and extracellular matrix proteins through macropinocytosis, suggesting that the α-actinin proteins can regulate multiple tumor cell properties through this endocytic process. In summary, these data demonstrate a critical role for the α-actinin isoforms in tumor cell macropinocytosis, thereby affecting the growth and invasive potential of PDAC tumors.

Monitoring Editor
Diane Barber
University of California, San Francisco

Received: Dec 8, 2020
Revised: May 5, 2021
Accepted: May 12, 2021

This article was published online ahead of print in MBoC in Press (http://www.molbiolcell.org/cgi/doi/10.1091/mbc.E20-12-0755) on May 19, 2021.

*Address correspondence to: Gina L. Razidlo (razidlo.gina@mayo.edu); Mark A. McNiven (mcniven.mark@mayo.edu).

Abbreviations used: ATP, adenosine triphosphate; BSA, bovine serum albumin; CaCl2, calcium chloride; DAPI, 4′,6-diamidino-2-phenylindole; DMEM, Dulbecco's modified eagle's medium; DPBS, Dulbecco's phosphate-buffered saline; DQ-collagen, dye quenching collagen; ECM, extracellular matrix; EGFR, epidermal growth factor; EGTA, ethylene glycol-bis(β-aminoethyl ether)-*N*,*N*,*N*′,*N*′-tetraacetic acid; EIPA, 5-(*N*-ethyl-*N*-isopropyl)-Amiloride FAK, focal adhesion kinase; FBS, fetal bovine serum; FITC, Fluorescein isothiocyanate; FRAP, fluorescence recovery after photobleaching; G-actin, globular actin; GFP, green fluorescent protein; HBSS, Hanks' Balanced Salt Solution; HPDE, human pancreatic ductal epithelial; IRB, institutional review board; KCl, potassium chloride; Keratinocyte-SFM, serum free media; LSM, laser scanning microscopy; $MgCl_2$, magnesium chloride; $MgSO_4$, magnesium sulfate; MTT, 3-(4,5-dimethylthiazol-2-yl)-2,5-diphenyltetrazolium bromide; N-PTX, nab-paclitaxel; NaN_3, sodium azide; Opti-MEM, minimal essential media; PCR, polymerase chain reaction; PDAC, pancreatic ductal adenocarcinoma; PDX, patient derived xenograft; PIPES, piperazine-*N*,*N*′-bis(2-ethanesulfonic acid); PM-mCherry, plasma membrane tethered mCherry; RNA, ribonucleic acid; SDS-PAGE, sodium dodecyl sulphate–polyacrylamide gel electrophoresis; SEM, standard error of the mean; siRNA, small interfering ribonucleic acid; TMR, tetramethylrhodamine.

INTRODUCTION

Pancreatic ductal adenocarcinoma (PDAC) is one of the most lethal tumor types due in large part to the aggressive nature of the disease and high rates of metastasis (Siegel *et al*., 2018; Orth *et al*., 2019). Recent studies suggest that alterations in tumor cell metabolism are largely responsible for providing the energy required to drive tumor cell proliferation and invasion (Roy *et al*., 2015; Elia *et al*., 2018; Labuschagne *et al*., 2019; Papalazarou *et al*., 2020). Activating mutations in the oncogene KRAS, which occur in more than 90% of PDAC patients, drive multiple changes in the utilization of metabolic pathways in PDAC cells to promote tumor cell survival (Ying *et al*., 2012; Bryant *et al*., 2014; Waters and Der, 2018; Buscail *et al*., 2020). One recently described mechanism up-regulated by KRAS in PDAC cells is macropinocytosis, the nonselective internalization of extracellular material through membrane ruffling and vesicle formation (Commisso *et al*., 2013; Kamphorst *et al*., 2015; Bloomfield and Kay, 2016). This pathway has been described to be utilized by tumor cells to internalize a diverse collection of material, including albumin, extracellular matrix (ECM) proteins, and exosomes, which have been shown to provide energy to support tumor cell proliferation (Qian *et al*., 2014; Zhao *et al*., 2016; Olivares *et al*., 2017; Kim *et al*., 2018). Additionally, macropinocytosis is being investigated as a

mechanism by which chemotherapeutics could be delivered more specifically to tumor cells and reduce off-target effects on healthy cells (Ha *et al.*, 2016; Kamerkar *et al.*, 2017). Understanding the machinery that drives macropinocytosis in PDAC cells will provide more direction in designing therapies for selective uptake and targeting of tumor cells.

Macropinocytosis is dependent on cytoskeletal remodeling at the plasma membrane to induce the formation of structures called dorsal ruffles that form the beginning of a macropinosome. Ras signaling cascades lead to activation of the Rho GTPase Rac1, initiating actin polymerization and formation of branched actin networks that provide structure for remodeling of the plasma membrane (Swanson, 2008; Fujii *et al.*, 2013; Buckley *et al.*, 2020). One family of proteins important for stabilizing branched actin networks are the α-actinin proteins, which are actin-bundling proteins that stabilize the actin cytoskeleton in structures like lamellipodia and focal adhesions (Sjoblom *et al.*, 2008; Murphy and Young, 2015). α-Actinin 1 and α-actinin 4 represent the nonmuscle isoforms of the actinin family expressed in most cell types, and they function as homo- or heterodimers to simultaneously bind and stabilize two actin filaments (Foley and Young, 2014). In macrophages, where macropinocytosis is a constitutive process, α-actinin 4 was shown to localize to membrane ruffles where macropinosomes are internalized (Araki *et al.*, 2000). Additionally, a recent full-genome small interfering RNA (siRNA) screen of proteins involved in HRAS-driven macropinocytosis in HeLa cells revealed a collection of actin-related proteins that were required for this process, including α-actinin 4 (Ramirez *et al.*, 2019). While these pieces of evidence point toward a role for α-actinin 4 in macropinocytosis, the role of the two nonmuscle α-actinin isoforms has not been studied in KRAS-driven macropinocytosis of PDAC cells, and the molecular function of these proteins during this process remains poorly defined.

α-Actinin 4 is overexpressed in multiple types of cancer, including PDAC (Honda *et al.*, 2005; Honda, 2015; Yamamoto *et al.*, 2007; Kikuchi *et al.*, 2008; Welsch *et al.*, 2009; Shao *et al.*, 2014; Wang *et al.*, 2015; Surcel *et al.*, 2019), while α-actinin 1 has been implicated less frequently in cancer progression (Kovac *et al.*, 2018; Yang *et al.*, 2019; Xie *et al.*, 2020). α-Actinin 4 enhances tumor cell migration and invasion through regulating focal adhesion formation and the stabilization of invasive protrusions called invadopodia to degrade the ECM during PDAC cell invasion (Fukumoto *et al.*, 2015; Yamaguchi *et al.*, 2017; Burton *et al.*, 2020). Overexpression of α-actinin 4 in PDAC is associated with decreased survival of patients (Kikuchi *et al.*, 2008; Welsch *et al.*, 2009; Burton *et al.*, 2020), so understanding how α-actinin 4 enhances the aggressiveness of PDAC will provide useful information about how to best treat this highly metastatic disease.

While the α-actinin proteins are critical regulators of tumor cell migration by controlling the actin cytoskeleton, there has been limited investigation into how the actinins may also influence tumor cell growth or nutrient uptake through cytoskeletal regulation during macropinocytosis. It was reported that knockdown of α-actinin 4 in orthotopically transplanted tumor cells in immunodeficient mice impaired growth (Kikuchi *et al.*, 2008), but the mechanism has not been studied. α-Actinin 4 is overexpressed in primary PDAC tumors, so this overexpression of α-actinin 4 may be providing a growth advantage to the primary PDAC tumor. In addition, the conservation of machinery between tumor cell growth and metastasis would provide a useful mechanism by which tumor cells could coordinate nutrient uptake and energy production with invasion during the metastatic process. To this end, we hypothesized that the α-actinin proteins were involved in the regulation of macropinocytosis in PDAC cells and through this could impact tumor growth. In this study, we first identify isoform-specific roles for the α-actinin proteins in macropinocytosis. We observe that α-actinin 4 is required for membrane ruffling to form the macropinosome, while α-actinin 1 is required for trafficking of macropinosomes to the acidic lysosome for degradation. Using a model of tumor cell growth dependent on uptake of extracellular protein, we then show that the function of the α-actinin isoforms in macropinocytosis is required for optimal cell growth, supporting a role for these actin cross-linking proteins in tumor progression. Additionally, we extend the role of the α-actinin proteins in PDAC cell macropinocytosis to functional outcomes other than nutrient uptake, including uptake of the albumin-bound chemotherapeutic nab-paclitaxel (N-PTX), as well as the uptake of ECM proteins like collagen, which could support invasive migration during metastatic dissemination from the primary tumor. Together, these observations demonstrate a role for the α-actinin proteins in growth-promoting processes in tumor cells and link cell growth and invasion through the coordination of the actin cytoskeleton.

RESULTS

α-Actinin 1 and 4 contribute to enhanced cell viability by supporting macropinocytosis

We previously reported that both α-actinin 1 and 4 are expressed in the neoplastic ducts in primary PDAC tumors and patients with high α-actinin 4 expression had decreased survival compared with patients with low α-actinin 4 expression (Burton *et al.*, 2020). While we previously focused on the role of α-actinin 4 in tumor cell invasion through the function of invadopodia, we were interested in determining whether the expression of α-actinin 1 and 4 in the primary PDAC tumors was important for tumor cell growth. The chromosomal locus where the α-actinin 4 gene resides is known to undergo an amplification event in PDAC which drives increased α-actinin 4 expression (Kikuchi *et al.*, 2008), so the α-actinin proteins may be important for tumor progression before metastasis. To further define the role of the actinins in PDAC growth and metastasis, we performed additional immunohistochemical staining of PDAC and normal pancreas tissue sections to compare the expression of α-actinin 1 and 4 with a widely used indicator of cell proliferation, Ki-67, and an indicator of enhanced KRAS activity and macropinocytosis, phosphorylated ERK. While pancreatic acinar cells expressed low to moderate levels of all these proteins, a markedly increased expression of both α-actinin isoforms as well as Ki-67 and p-ERK was observed in the neoplastic ducts, suggesting a functional correlation (Figure 1A). To directly test for a role of α-actinin 1 and 4 in cell proliferation and viability, cultured human PDAC cells (MIA PaCa-2 and Dan-G), as well as the benign human pancreatic ductal epithelial (HPDE) cell line, were subjected to siRNA knockdown of α-actinin 1 or 4 and cultured for 5 d, followed by a 3-(4,5-dimethylthiazol-2-yl)-2,5-diphenyltetrazolium bromide (MTT) assay. As depicted in Figure 1, B and C, knockdown of either α-actinin isoform reduced the growth of the PDAC tumor cells by 40–50% over the 5 day growth period compared with control treated cells (Figure 1, B and C). We observed a similar 30–40% decrease in cell viability after knockdown of α-actinin 1 or 4 in the normal HPDE cells, reinforcing the concept of an important role for the α-actinin proteins in proliferation (Supplemental Figure 1A). These data suggest that in addition to regulating tumor cell invasion (Fukumoto *et al.*, 2015; Yamaguchi *et al.*, 2017; Burton *et al.*, 2020), the expression of the nonmuscle α-actinin isoforms in the primary PDAC tumor may provide a proliferative advantage.

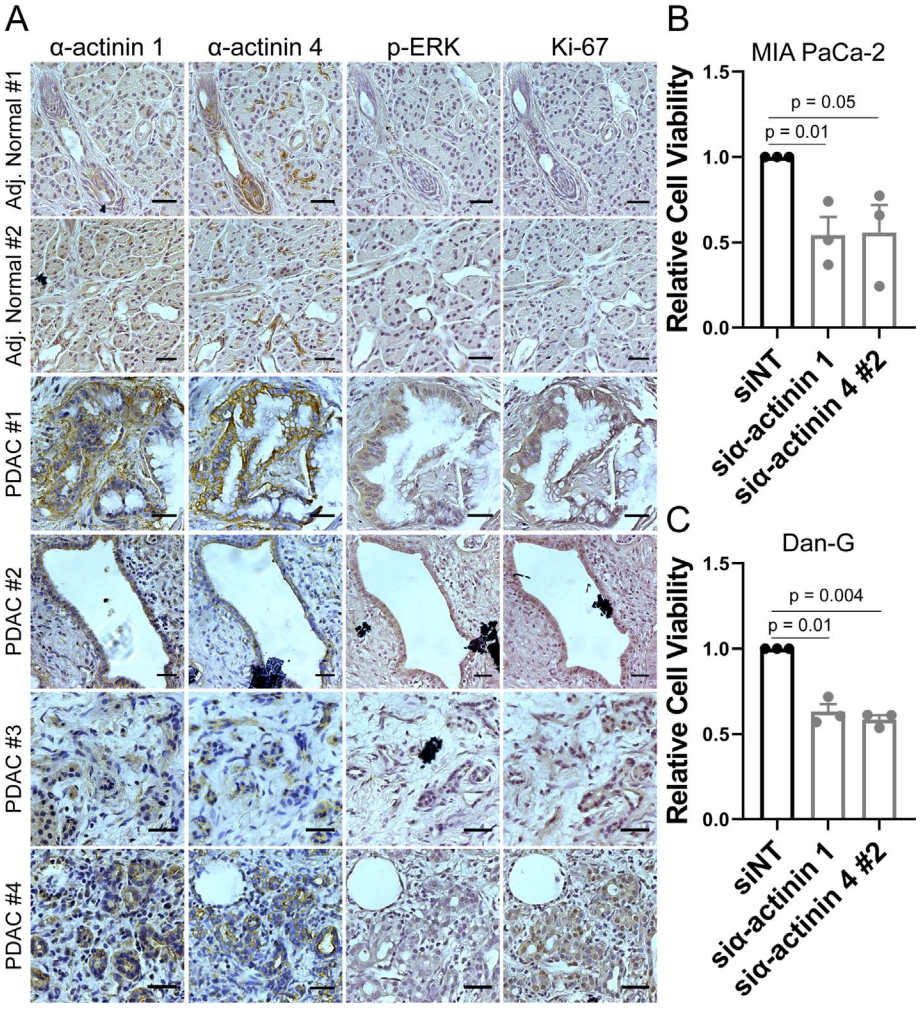

FIGURE 1: α-Actinin 1 and 4 show increased expression in patient PDAC tumors and correlate with tumor cell viability. (A) Immunohistochemical staining of human primary PDAC and adjacent normal tissue sections stained for α-actinin 1 and 4 as well as markers for proliferation (Ki-67) and cells with high KRAS activity (p-ERK Thr 202/Tyr 204). (B, C) MTT cell viability assays were performed in MIA PaCa-2 (B) and Dan-G (C) cells after 5 day on cells treated with siRNA against α-actinin 1 or 4. Graphed data represent the mean ± SEM for three independent experiments. Scale bars: 20 μm (A). A two-tailed Student's *t* test was used to measure statistical significance, and significant *p* values are shown above the graphs.

The actin cytoskeleton plays a central role in macropinocytosis, a process now well-defined to provide tumor cells with a nutritional source (Commisso *et al.*, 2013; Bloomfield and Kay, 2016). As the α-actinins participate in the regulation of actin dynamics, we tested whether these proteins might play an important role in tumor cell macropinocytosis. To follow macropinocytosis in PDAC cells in culture, we expressed a form of mCherry tethered to the plasma membrane (PM-mCherry) that uses the N-terminal 10 amino acids in Lyn kinase that are sites for myristoylation and palmitoylation to drive insertion into the plasma membrane. This probe was used previously to study macropinocytosis in cultured cells as it labels membrane ruffles and plasma membrane–derived vesicles (Corbett-Nelson *et al.*, 2006; Dolat and Spiliotis, 2016). Expression of PM-mCherry in human 6741 pancreatic cancer cells, which were cultured from a patient-derived xenograft, or in MIA PaCa-2 cells revealed high levels of membrane ruffling and vesicle internalization consistent with macropinocytosis. Further, green fluorescent protein (GFP)-tagged forms of either α-actinin 1 or α-actinin 4 showed marked localization to both dynamic membrane ruffles and the surface of internalizing macropinosomes (Figure 2, A–D; Supplemental Videos 1 and 2). When normalized to PM-mCherry, both α-actinin 1 and α-actinin 4 localization to membrane ruffles was enriched by 50–80% compared with nonruffling regions within each cell (Figure 2, E and F).

To test the requirement of the two α-actinin isoforms in PDAC macropinocytosis, we measured the uptake of the macropinocytic cargo 70 kDa tetramethylrhodamine (TMR)-dextran in cells following siRNA-mediated knockdown of either α-actinin protein. As a control, cells were treated with the Na^+/H^+ transporter inhibitor 5-(*N*-ethyl-*N*-isopropyl)-Amiloride (EIPA) (Figure 2, G and H), known to attenuate macropinocytosis through disruption of the pH near the plasma membrane, leading to impaired actin remodeling (Koivusalo *et al.*, 2010). While both α-actinin isoforms localize to the site of macropinosome internalization, we observed that knockdown of α-actinin 4 significantly reduced dextran uptake by 80% in MIA PaCa-2 cells, while knockdown of α-actinin 1 led to only a modest decrease in dextran uptake (Figure 2, G, H, and M). Similar effects were observed in two additional PDAC cell lines (Dan-G and CFPAC-1: Supplemental Figure 1, C–E and F–H) and with an additional siRNA against α-actinin 4 (Supplemental Figure 1, I–K). These PDAC cell lines were chosen for study based on having the most robust uptake of dextran among the eight cell lines tested. Additional knockdown experiments using a second widely used macropinocytosis cargo, TMR-tagged bovine serum albumin (BSA), were also performed and again showed a strong requirement for the presence of α-actinin 4 compared with that of α-actinin 1 (Figure 2, I and J). Knockdown of α-actinin 4 reduced BSA uptake by 70%, where knockdown of α-actinin 1 more modestly reduced uptake by 30%. Finally, this dependence on α-actinin 4 versus α-actinin 1 was also observed in manipulated tumor cells challenged to internalize a labeled ECM protein, DQ-collagen, which fluoresces upon cleavage (Figure 2, K and L). Here, depletion of α-actinin 4 nearly completely blocked uptake of cleaved collagen, where reduction of α-actinin 1 had no effect. Taken together these findings support a differential requirement for a specific α-actinin, α-actinin 4, during the macropinocytic internalization of nutritional components.

α-Actinin 4 promotes cortical actin dynamics to drive macropinocytosis

To address the mechanism by which α-actinin 4 mediates macropinocytosis in PDAC cells, we first investigated the effects of α-actinin knockdown on actin dynamics. To this end, live cell imaging was performed using the actin probe LifeAct-mCherry in MIA PaCa-2 cells treated with siRNA against either α-actinin 1 or 4, and the

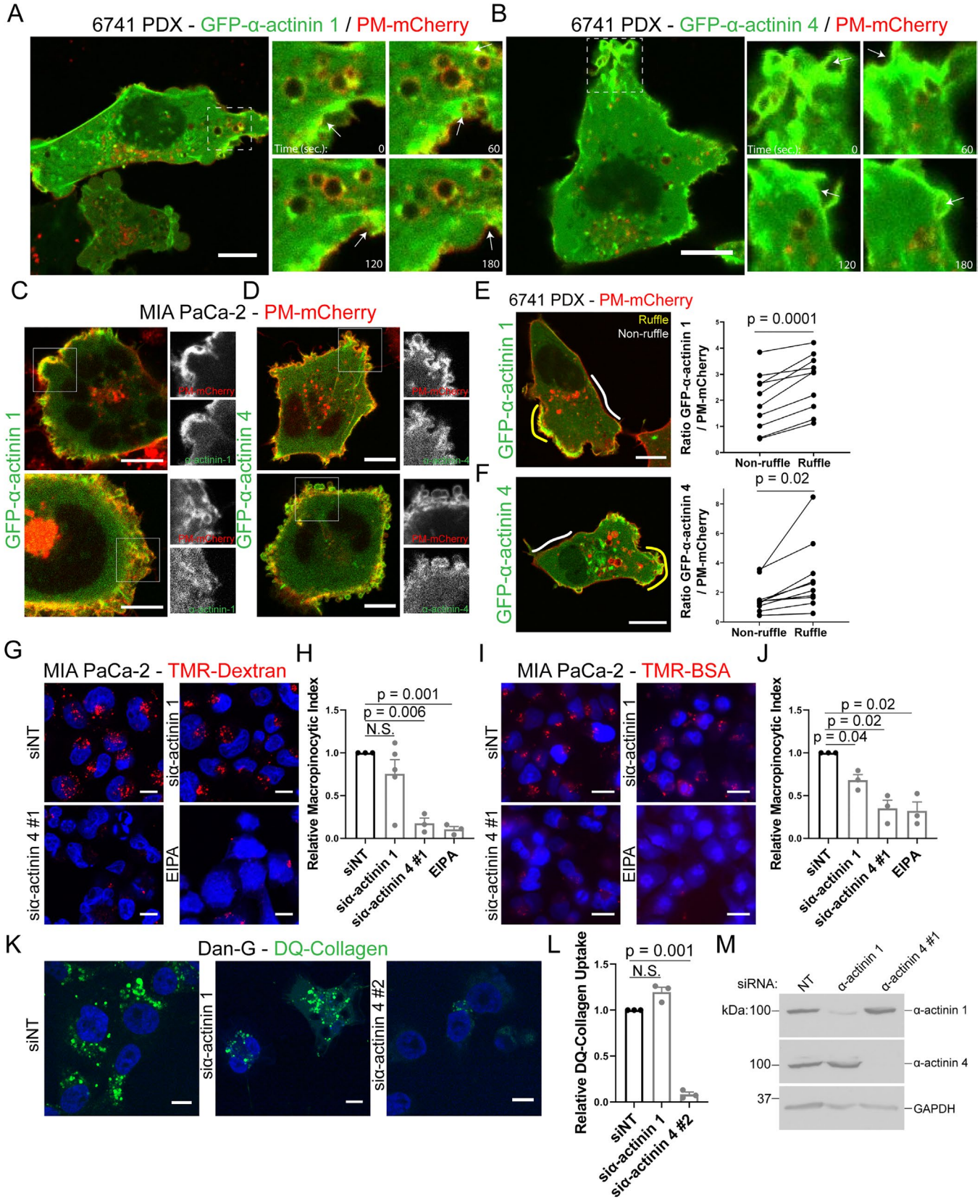

FIGURE 2: α-Actinin 4, but not α-actinin 1, is required for uptake of macropinosomes in PDAC cells. (A, B) Live cell imaging of 6741 PDX cells expressing either GFP-α-actinin 1 (A) or GFP-α-actinin 4 (B) with PM-mCherry was performed to visualize membrane ruffling and macropinosome internalization. Arrows indicate α-actinin–positive membrane ruffles where PM-mCherry–positive macropinosomes are internalized. (C, D) Live cell imaging of MIA PaCa-2 cells expressing either GFP-α-actinin 1 (C) or GFP-α-actinin 4 (D) with PM-mCherry confirms that the α-actinin isoforms localize to

percentage of cells that exhibited stress fibers or membrane ruffles was quantified. In control cells, membrane ruffles were observed in approximately 40–50% of cells while few stress fibers were observed, consistent with a dynamic actin cortex that supports macropinocytosis. Importantly, actin organization was severely altered in α-actinin 4 knockdown cells, with most cells exhibiting significantly less actin dynamics and membrane ruffling while accumulating robust cortical actin and large stress fiber–like structures along the cell periphery (Figure 3, A–C; Supplemental Videos 3–5). This reduction in actin dynamics was also observed in Dan-G cells, where the number of cells exhibiting membrane ruffles decreased from 60% in control cells to 30% after α-actinin 4 knockdown (Supplemental Figure 2, A–C). In contrast, cells that were treated with siRNA to reduce endogenous α-actinin 1 showed little change in actin organization or dynamics in both PDAC cell lines.

Our analysis of actin dynamics was extended by methods to quantify actin incorporation and turnover at the plasma membrane. While the α-actinin isoforms act as known actin cross-linking proteins, they can also indirectly influence the formation of actin networks primarily through an interaction with the Arp 2/3 actin nucleating complex. Further, altering the expression of α-actinin can impact the formation of actin networks at sites such as the cortical cytoskeleton and at focal adhesions (Mukhina *et al.*, 2007; Tang and Brieher, 2012; Pizarro-Cerda *et al.*, 2017). Therefore, it seemed plausible that a loss of α-actinin 4 might impair macropinocytosis and membrane ruffling by limiting the ability of the cells to reorganize the actin cytoskeleton on the plasma membrane during this highly dynamic process. Fluorescence recovery after photobleaching (FRAP) analysis was performed in MIA PaCa-2 cells expressing GFP-β-actin to measure the rate of actin treadmilling in the cortical actin cytoskeleton associated with the plasma membrane. Cortical GFP-β-actin was photobleached, and the recovery of actin to these regions was monitored for 50 s. There was a significant decrease of the GFP-β-actin FRAP in cells following knockdown of α-actinin 4. In comparison, cells with reduced α-actinin 1 did not exhibit a decrease in the FRAP of GFP-β-actin at the plasma membrane (Figure 3, D–F and H–J). We also measured the recovery half-times of GFP-β-actin on the plasma membrane and, while a statistical difference was not observed, we found that knockdown of α-actinin 1 tended to lead to faster recovery of actin. This again suggests that the actin-binding affinity and the roles of the two α-actinin isoforms in organization of the actin cytoskeleton are distinct from each other in PDAC cells (Figure 3, G and K). This also implicates α-actinin 4 in dynamic actin treadmilling at the plasma membrane.

We additionally tested the requirement for α-actinin in the incorporation of actin into growing filaments by performing actin nucleation assays with rhodamine G–actin following knockdown of α-actinin 1 or 4 (Chan *et al.*, 1998, 2000). In control cells, we observed significant incorporation of rhodamine G–actin into the cortical cytoskeleton where membrane ruffling would be occurring. However, after knockdown of α-actinin 4 we observed a 40% decrease in rhodamine G–actin fluorescence and much less incorporation of the fluorescent actin into the cortical cytoskeleton. Knockdown of α-actinin 1 resulted in a more modest 25% decrease in rhodamine G–actin incorporation (Figure 3, L and M). These findings suggest that α-actinin 4 preferentially regulates cortical actin dynamics that can, in turn, support macropinocytotic uptake of cargo.

α-Actinin 1 regulates macropinosome trafficking to the lysosome for degradation of cargo

Though α-actinin 4 has a more prominent role in regulating macropinocytic uptake, live cell imaging revealed localization of both α-actinin 1 and 4 to macropinosomes following internalization and suggested that they may remain associated with macropinosomes during transport through the cytoplasm (Figure 2, A and B). As an alternate method to visualize this process, live cell imaging of GFP-α-actinin 1 and 4 was performed in cells loaded with TMR-dextran to visualize movement of the macropinosomes postinternalization. Both α-actinin isoforms can be observed on numerous TMR-dextran–positive vesicles in the cytoplasm (Figure 4, A and B; Supplemental Videos 6 and 7), suggesting that the role of α-actinin in macropinocytosis may extend beyond the internalization at the plasma membrane. The polarized orientation of GFP-α-actinin 1/4 on macropinosomes suggested that these structures may represent actin comet tails, which are made up of bundled actin filaments that undergo active treadmilling to push the associated vesicle forward through the cytoplasm (Orth *et al.*, 2002; Fehrenbacher *et al.*, 2003). Analysis of the movement of individual macropinosomes using the TrackMate plug-in in ImageJ revealed that the GFP-α-actinin 1/4 tails on macropinosomes were oriented toward the rear of the vesicle during trafficking, which suggests that these GFP-α-actinin 1/4 tails may be involved in the propulsion of macropinosomes (Figure 4, A and B). Subsequent imaging of these cells expressing GFP-α-actinin 1 or 4 and LifeAct-mCherry, to follow real time actin dynamics, revealed polarized tufts of newly assembled actin with associated GFP-α-actinin 1/4 upon the translocating macropinosomes loaded with Alexa 647–labeled N-PTX, another macropinocytic cargo in PDAC cells (Supplemental Figure 3, A and B). The requirement for α-actinin 1 in the formation of these actin comets was tested using live cell imaging of MIA PaCa-2 cells expressing GFP-LifeAct to mark the actin cytoskeleton after macropinocytic uptake

membrane ruffles. (E, F) Line scan analysis of GFP-α-actinin 1 (E) or GFP-α-actinin-4 (F) fluorescence relative to PM-mCherry fluorescence was quantified in membrane ruffle (yellow lines) and static plasma membrane regions (white lines) in 10 cells across three experiments. Graphs show paired measurements within cells to control for levels of protein expression, and statistical analysis was performed using a paired *t* test. (G, H) TMR-dextran uptake assays were performed in MIA PaCa-2 cells by incubating cells with 1 mg/ml TMR-dextran for 20 min, followed by fixation and DAPI staining. The macropinocytic index was calculated as (area of dextran/total cell area) × 100 and normalized to the siNT control. (I, J) TMR-BSA uptake assays were performed in MIA PaCa-2 cells as described previously for TMR-dextran. (K, L) Dan-G cells were plated on coverslips coated with collagen and DQ-collagen for 16 h, and the amount of DQ-collagen internalized into the cells was quantified. (M) Western blot showing the knockdown efficiency of the α-actinin 1 and 4 siRNAs in MIA PaCa-2 cells. Scale bars: 10 μm. Graphed data represent the mean ± SEM, and plotted data points represent average values for individual experiments, with at least three independent experiments performed. A total of 10 40× fields of cells were quantified for each condition per experiment for all macropinocytic uptake assays. A two-tailed unpaired Student's *t* test (and paired *t* test for Figure 2, E and F) was used to measure statistical significance, and significant *p* values are shown above the graphs.

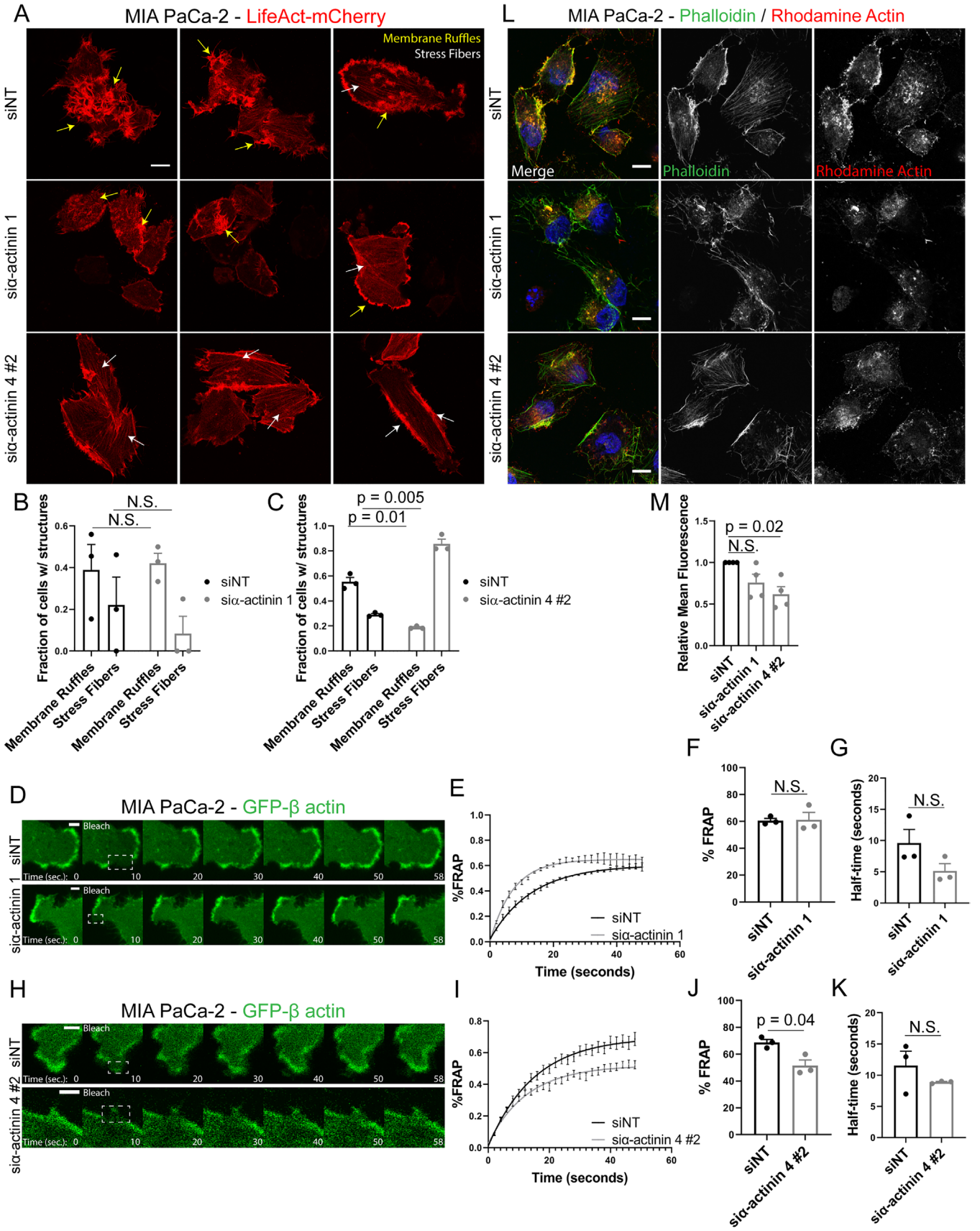

FIGURE 3: α-Actinin 4 supports cortical actin dynamics to generate membrane ruffles during macropinocytosis. (A–C) The number of cells exhibiting membrane ruffles and stress fibers was quantified from live cell movies of MIA PaCa-2 cells expressing LifeAct-mCherry after knockdown of α-actinin 1 (B), which did not impact actin dynamics, or α-actinin 4 (C), which reduced membrane ruffling and enhanced stress fiber formation. Between 37 and 52 cells were

of TMR-dextran. We observed a significant decrease in the number of dextran vesicles positive for GFP-LifeAct tails in the α-actinin 1 knockdown cells, indicating that α-actinin 1 supports the stabilization of these structures (Figure 4, C and D). It was not possible to test the requirement for α-actinin 4 in comet formation on macropinosomes, as macropinosome internalization was markedly reduced following α-actinin 4 knockdown (Figure 2). The velocity of the internalized macropinosomes was also tested, but no differences following α-actinin 1 knockdown were observed, suggesting that while α-actinin 1 may be required for actin comet formation, it does not control trafficking velocity (Figure 4E). Of note, it is possible that α-actinin 4 may be able to compensate for the loss of α-actinin 1 in these experiments. These findings are consistent with the premise that the α-actinin proteins localize to actin comets.

As the role of actin comets is to facilitate vesicle trafficking, we tested whether α-actinin 1 was required for macropinosome trafficking to the lysosome, where its contents are degraded. To assess macropinosome trafficking to the terminal endocytic compartment, we first measured the amount of colocalization with lysosomes labeled with Lysotracker Blue following TMR-dextran loading and a chase in label-free media for 0 or 120 min. A 50% increase in colocalization between TMR-dextran and Lysotracker was observed following the 120-min chase in control cells, consistent with trafficking to the lysosome. Importantly, in the α-actinin 1 knockdown cells, there was no noticeable increase in colocalization between TMR-dextran and Lysotracker between the 0 and 120 min time points, indicating a defect in lysosomal targeting (Figure 4, F and G). An additional strategy was employed in which cells were concomitantly labeled with both TMR-dextran, as a general macropinosome marker, and DQ-BSA, which fluoresces only upon cleavage within the acidic lysosome. The appearance of DQ-BSA fluorescence would indicate targeting of the internalized macropinosomes to the lysosome. DQ-BSA was confirmed to mark acidic lysosomes as more than 90% colocalization with Lysotracker was observed (Supplemental Figure 3, F and G). We next tested whether α-actinin 1 was required for lysosomal accumulation and fluorescence of DQ-BSA. Following macropinocytic uptake, cells were chased in TMR-dextran and DQ-BSA–free media for 0–120 min to allow for internalization and trafficking of macropinosomes, and then the cells were imaged and the TMR-dextran and DQ-BSA fluorescence was measured. Control MIA PaCa-2 cells showed an appreciable increase in DQ-BSA emittance within dextran-positive lysosomes by 60–120 min, suggesting an active transfer of cargo from the macropinosome to the lysosome. As predicted, α-actinin 1 knockdown did not affect macropinosome internalization as measured by TMR-dextran uptake (Figure 4, H and I). However, cells with reduced α-actinin 1 exhibited a 30% reduction in DQ-BSA fluorescence after the 120 min chase, suggesting a decreased efficiency in the trafficking of macropinosomes to the lysosome (Figure 4, H and J). A similar outcome was observed in Dan-G cells (Supplemental Figure 3, C–E). To ensure that the reduced DQ-BSA signal was not due to decreased lysosome acidity in cells depleted for α-actinin 1, the pH-sensitive Lysotracker dye was utilized as a control and showed no reduction in the number or intensity of lysosomes in control versus α-actinin 1 knockdown cells (Figure 4, K and L). Taken together these findings suggest that α-actinin 1, while not essential for macropinosome internalization, is required for the trafficking of macropinosomes to the lysosome in PDAC cells.

α-Actinin 1/4 are required for macropinocytosis-derived nutrient uptake and proliferation

Macropinocytosis of extracellular material has been shown to support PDAC cell proliferation by supplying tumor cells with additional nutrients to support high metabolic demands (Commisso *et al.*, 2013; Kamphorst *et al.*, 2015; Olivares *et al.*, 2017). The observations described above indicate that both α-actinin isoforms are involved in the formation, uptake, and trafficking of macropinosomes to the lysosome for degradation and therefore could play a central role in tumor cell proliferation. To this end, cell viability assays were utilized to test the requirement of tumor cells taking up BSA through macropinocytosis to support cell growth in low nutrient conditions (Commisso *et al.*, 2013). In this assay, cells were cultured in low-glutamine media to suppress growth, with the addition of 3% BSA stimulating proliferation by providing a glutamine source that can be catabolized through macropinocytosis and lysosomal degradation. This assay was used to test whether experimentally induced reduction of either α-actinin isoform would block BSA-stimulated growth. Importantly, knockdown of α-actinin 4, which inhibits macropinocytosis (Figure 2), or α-actinin 1, which decreases macropinosome trafficking to the lysosome (Figure 4), markedly decreased the response of tumor cells to exogenous BSA as compared with control cells (Figure 5, A and B). This indicates that the high proliferative capacity of PDAC cells is at least in part reliant on the role of the α-actinin isoforms in the uptake and trafficking of extracellular material to the lysosome as a nutritional source.

It is now known that conjugating chemotherapeutics to large carriers such as albumin, exosomes, or liposomes facilitates specific uptake of drugs into tumor cells through macropinocytosis (Liu *et al.*, 2019; Liu and Ghosh, 2019). N-PTX is an albumin-conjugated form of paclitaxel that is used to treat pancreatic cancer, in combination with gemcitabine (Von Hoff *et al.*, 2013; Al-Batran *et al.*, 2014; Rajeshkumar *et al.*, 2016). N-PTX exhibits increased stability in the circulation and is more efficient at inducing PDAC cell death than paclitaxel alone. We first tested whether N-PTX is internalized by

quantified per condition. White arrows indicate stress fibers, and yellow arrows indicate membrane ruffles. (D–K) FRAP of the cortical actin cytoskeleton was performed in MIA PaCa-2 cells expressing GFP-β-actin after knockdown of α-actinin 1 (D–G) or α-actinin 4 (H–K), which significantly reduced FRAP of cortical actin. Plasma membrane regions were imaged for 10 s before photobleaching, and GFP-β-actin recovery was measured for 50 s. Three plasma membrane regions in 18 cells were analyzed per condition. Percent FRAP (F, J) was calculated as the average percentage of actin fluorescence recovered, using prebleach fluorescence as 100% and the frame after bleaching as 0% (E, I). Half-time values for the recovery of GFP-β-actin fluorescence were calculated using nonlinear regression analysis of the FRAP curves in E and I (G, K). (L–M) Rhodamine actin incorporation assays were performed by permeabilizing cells in the presence of 1 μM rhodamine G–actin for 15 min, followed by fixation. Cells were stained with FITC phalloidin (green) to label all actin filaments, while the rhodamine G–actin (red) shows newly incorporated actin, which is significantly decreased following knockdown of α-actinin 4. The relative mean fluorescence intensity of the rhodamine G–actin is plotted in M. A total of 10 40× fields of cells were quantified per condition for each rhodamine G–actin experiment. Scale bars: 10 μm (A, L), 3 μm (D, H). Graphed data represent the mean ± SEM, and plotted data points represent average values for individual experiments, with at least three independent experiments performed. Two-tailed Student's *t* test was used to measure statistical significance, and significant *p* values are shown above the graphs.

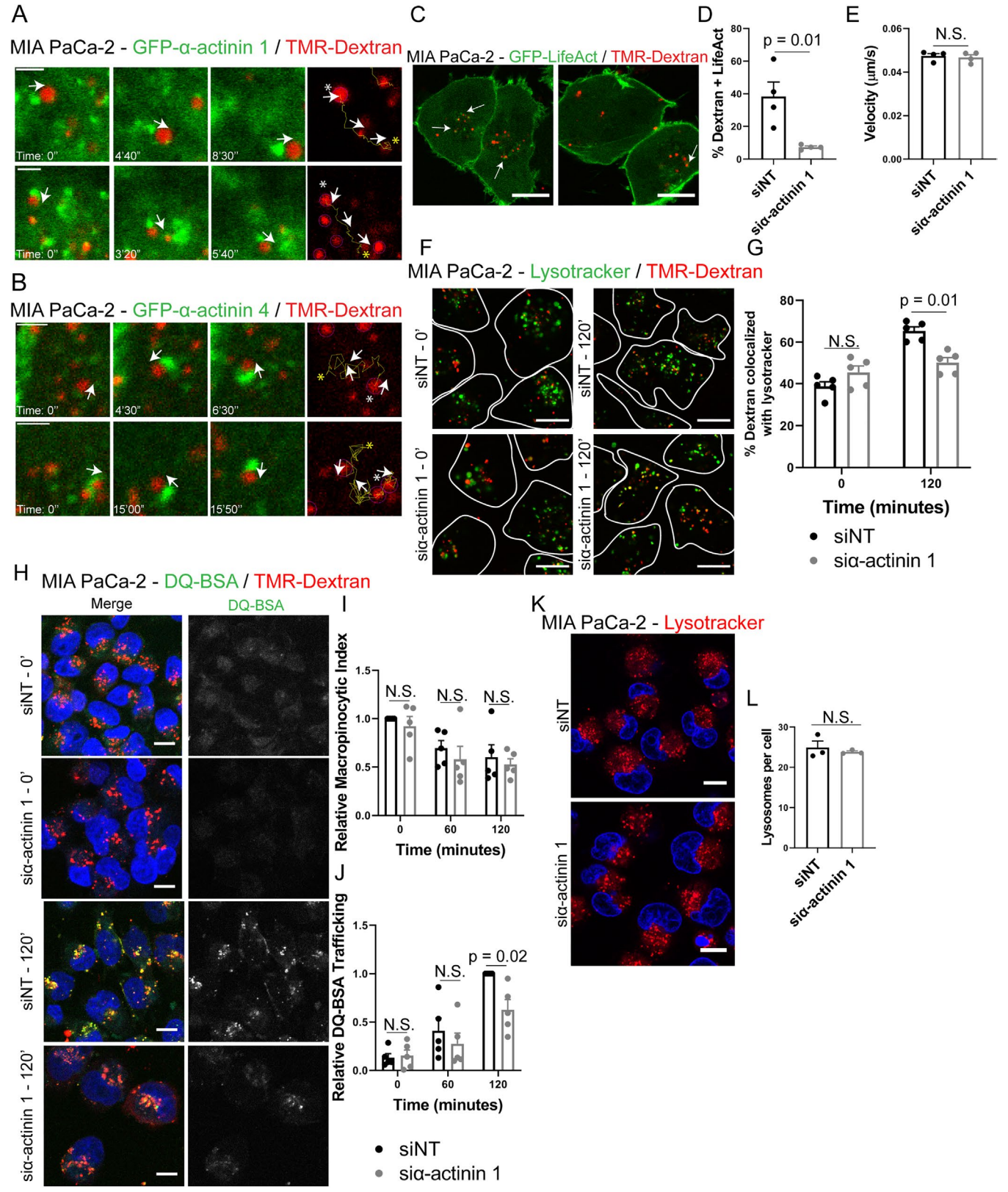

FIGURE 4: α-Actinin 1 participates in trafficking of macropinosomes to the lysosome for degradation. (A, B) Live cell imaging of MIA PaCa-2 cells expressing either GFP-α-actinin 1 (A) or GFP-α-actinin 4 (B) was performed after loading cells with TMR-dextran for 20 min to visualize trafficking of macropinosomes. TrackMate analysis was used to analyze the direction of macropinosome movement relative to the position of the α-actinin tail. The yellow line represents the track of movement of the course of imaging, marked by a white asterisk (start of track) and a yellow asterisk (end of track), and the arrows indicate the vector of movement of the dextran vesicle at the indicated time points, indicating that the α-actinin tails are positioned behind the moving macropinosome. (C–E) MIA PaCa-2 cells expressing

macropinocytosis in PDAC cells, as it has previously been reported to be internalized by macropinocytosis in macrophages (Cullis *et al.*, 2017) and other albumin-conjugated drugs have been shown to utilize this pathway for entry into tumor cells. N-PTX was conjugated to the far-red Alexa 647 dye in order to monitor its uptake and trafficking inside of tumor cells. After loading cells with both Alexa 647–N-PTX and the macropinocytosis cargo TMR-dextran, we observed extensive intracellular colocalization between the two cargoes, indicating they are both present in macropinosomes (Figure 5C). Further, treatment with the macropinocytosis inhibitor EIPA blocked uptake of Alexa 647–N-PTX, suggesting that N-PTX is internalized via macropinocytosis in tumor cells (Figure 5, D and E). Importantly, knockdown of α-actinin 4 also inhibited the uptake of N-PTX into tumor cells, consistent with the inhibition of uptake of the known macropinocytic cargoes dextran and BSA (Figure 5, D and E). Knockdown of α-actinin 1 did not affect N-PTX uptake in PDAC cells (Figure 5, D and E). These findings were also confirmed in Dan-G cells (Supplemental Figure 4, A and B). In addition, live cell imaging of GFP-α-actinin 1 or 4 in cells loaded with Alexa 647–N-PTX revealed that both α-actinin isoforms localized to N-PTX–filled vesicles as they trafficked inward post internalization (Figure 5, F and G). Both α-actinin isoforms localized to these vesicles to a similar extent, consistent with what we observed with dextran vesicles (Figure 4, A–D). Together these drug-based studies suggest that N-PTX is internalized and transported to the lysosome in PDAC cells through a macropinocytotic process supported in distinct ways by α-actinin 1 and 4. These findings suggest that macropinocytosis can also be utilized therapeutically as a way to deliver chemotherapeutics to tumor cells known to exhibit amplified macropinocytosis due to enhanced expression of the α-actinin proteins and other cytoskeletal regulators.

DISCUSSION

The actin cross-linking protein α-actinin is a well-established regulator of cell migration during tumor cell metastasis, and its overexpression in PDAC worsens patient prognosis. In this study, we identify that the α-actinin isoforms are able to sustain tumor cell growth via regulation of macropinocytosis. This includes not only regulation of the actin cytoskeleton during membrane ruffling to internalize macropinosomes (Figures 2 and 3), but also the formation of actin comets on macropinosomes that traffic these vesicles to the lysosome to release nutrients for cell growth (Figure 4). Via this process, α-actinin 1 and 4 impact not only tumor cell growth (Figure 5), but also uptake of chemotherapeutics (Figure 5) and internalization of ECM proteins during invasion (Figure 2). Together, these data highlight mechanisms by which the cytoskeletal remodeling machinery is able to impact a diverse number of tumor cell processes beyond cell migration and point toward new therapeutic vulnerabilities of PDAC cells that could inhibit tumor growth and metastasis simultaneously.

The α-actinin isoforms have unique functions during macropinocytosis, where α-actinin 4 is required for uptake (Figure 2) and α-actinin 1 may be more important for trafficking. While the two proteins are very similar by genetic sequence, the processes these proteins support may be quite different. Previous studies have identified functional differences between the α-actinin proteins during processes such as invadopodia formation, cell motility, adhesion, and the ability to translocate to the nucleus and act as a transcriptional coactivator (Babakov *et al.*, 2008; Quick and Skalli, 2010; Shao *et al.*, 2010; Fukumoto *et al.*, 2015; An *et al.*, 2016; Yamaguchi *et al.*, 2017; Burton *et al.*, 2020). There is, however, a lack of understanding of what facilitates these functional distinctions between the α-actinin isoforms, as they share the same domain structure. One possibility is that posttranslational modifications downstream of signaling pathways that drive these processes may act on only one isoform, as the α-actinin proteins have been shown to be modified by pathways such as EGFR and FAK signaling (Izaguirre *et al.*, 2001; Shao *et al.*, 2010). The α-actinin proteins also interact with a wide variety of proteins, which may separately drive their recruitment to discrete regions of the cell. There are also splice variants of the α-actinin proteins that affect their sensitivity to calcium, which could impact the actin-bundling activity of these proteins and change their function in the cell (Foley and Young, 2013). In addition, the α-actinin isoforms have been reported to have differential actin-binding affinities, which can be impacted by alternative splicing and indicates that α-actinin 1 has a much higher actin-binding affinity than α-actinin 4 (Meyer and Aebi, 1990; Murphy and Young, 2015; Rajeshkumar *et al.*, 2016; Morita *et al.*, 2020). Additionally, previous research has indicated that α-actinin 4 acts as a mechanosensitive actin-binding protein through its catch-slip activity that allows it to bind or release actin based on mechanical tension. This could potentially explain why we observe α-actinin 4 is more important for the dynamic actin remodeling in membrane ruffles (Xu *et al.*, 1998; Fukumoto *et al.*, 2015; Hosseini *et al.*, 2020). In addition, while we were interested in trafficking of macropinosomes to the lysosome as that provides nutrients to the proliferating tumor cells, the actinin proteins may also regulate recycling of material from macropinosomes back to the plasma membrane via interactions with other actin nucleating machinery such as WASH. Thus, additional roles and means of regulation could indicate multiple mechanistic

GFP-LifeAct were loaded with 1 mg/ml TMR-dextran for 20 min, followed by live cell imaging to measure actin comet tail formation and macropinosome velocity. The percentage of macropinosomes with GFP-LifeAct comet tails was quantified manually in 17–24 cells per condition, and macropinosome velocity was calculated using the TrackMate plug-in in ImageJ. (F, G) MIA PaCa-2 cells were loaded with 1 mg/ml TMR-dextran following treatment with the indicated siRNAs and chased in label-free media for 0 or 120 min and stained with Lysotracker Blue to measure trafficking of macropinosomes to the acidic lysosome. The percentage of dextran vesicles colocalized with Lysotracker was measured using ImageJ, and white lines indicate cell borders. (H–J) Monitoring the trafficking of macropinosomes to the lysosome was performed in MIA PaCa-2 cells by incubating cells with 1 mg/ml TMR-dextran and 0.5 mg/ml DQ-BSA for 20 min, followed by replacing the media and chasing for 0–120 min. The macropinocytic index for TMR-dextran representing macropinosome uptake (I) and the amount of DQ-BSA trafficked to the lysosome (J) were quantified across the different time points and show a reduction in DQ-BSA fluorescence after a 120 min chase in α-actinin 1 knockdown cells. (K, L) Lysosome number per cell was quantified in MIA PaCa-2 cells by labeling cells with Lysotracker Deep Red to label acidic endosomes. Scale bars: 2 μm (A, B), 10 μm (C, F, H, K). Graphed data represent the mean ± SEM, and plotted data points represent average values for individual experiments, with at least three independent experiments performed. A total of 10 40× fields of cells were quantified for each condition per experiment for all macropinosome trafficking (F–J) and lysosome number (K, L) assays. An unpaired two-tailed Student's *t* test was used to measure statistical significance, and significant *p* values are shown above the graphs.

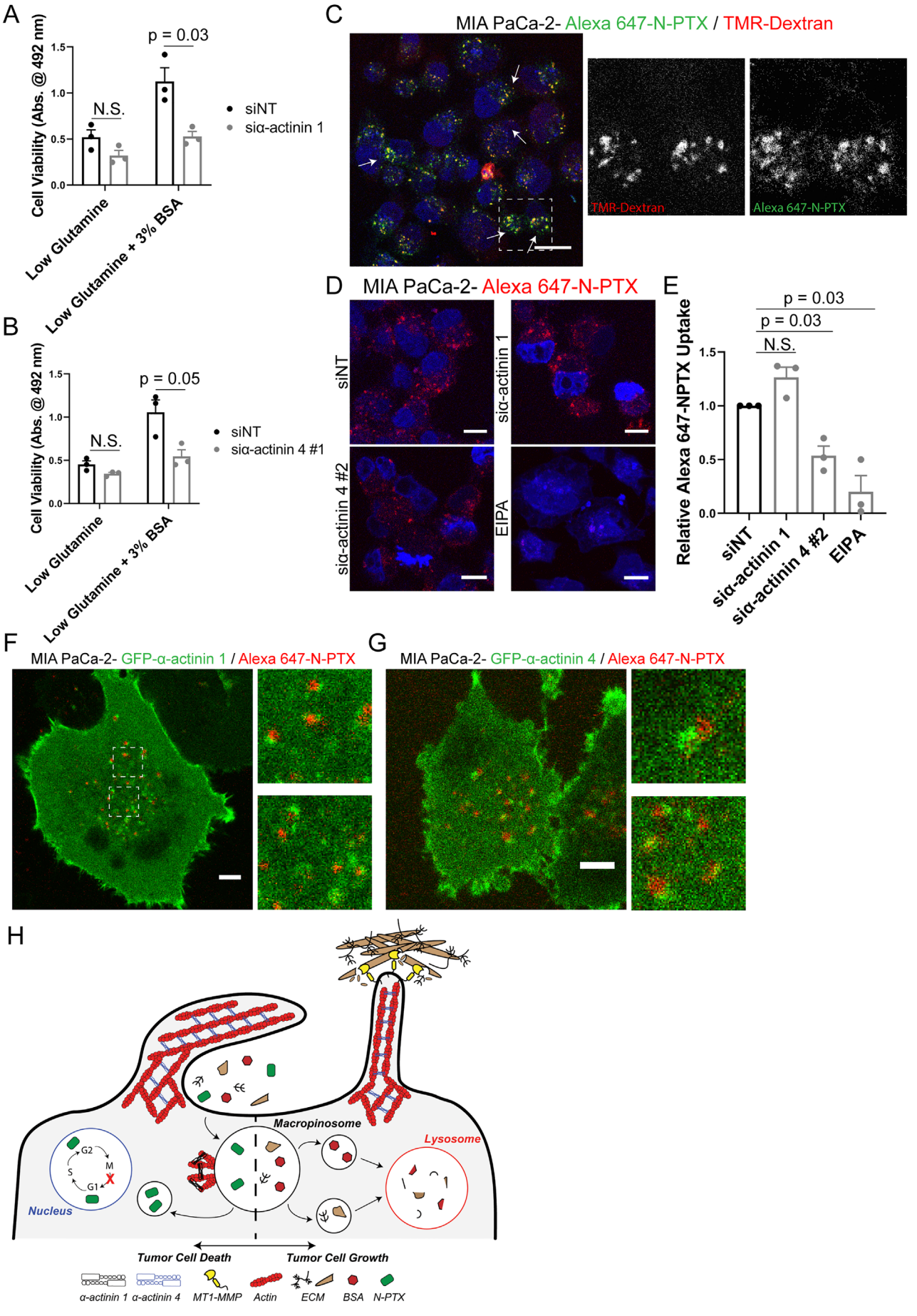
A
Cell Viability (Abs. @ 492 nm)
p = 0.03
N.S.
siNT
siα-actinin 1
Low Glutamine
Low Glutamine + 3% BSA
B
Cell Viability (Abs. @ 492 nm)
p = 0.05
N.S.
siNT
siα-actinin 4 #1
Low Glutamine
Low Glutamine + 3% BSA
C
MIA PaCa-2- Alexa 647-N-PTX / TMR-Dextran
TMR-Dextran
Alexa 647-N-PTX
D
MIA PaCa-2- Alexa 647-N-PTX
siNT
siα-actinin 1
siα-actinin 4 #2
EIPA
E
Relative Alexa 647-NPTX Uptake
p = 0.03
p = 0.03
N.S.
siNT
siα-actinin 1
siα-actinin 4 #2
EIPA
F
MIA PaCa-2- GFP-α-actinin 1 / Alexa 647-N-PTX
G
MIA PaCa-2- GFP-α-actinin 4 / Alexa 647-N-PTX
H
Macropinosome
Lysosome
Nucleus
G2
M
S
G1
Tumor Cell Death
Tumor Cell Growth
α-actinin 1
α-actinin 4
MT1-MMP
Actin
ECM
BSA
N-PTX

contributions by α-actinins toward macropinocytic uptake and subsequent trafficking. In addition to isoform-specific roles for these proteins, α-actinin 1 and 4 are able to heterodimerize, and while there is some evidence that this heterodimeric form may occur more frequently in tumor cell lines, the functions of this unique interaction are not well understood (Foley and Young, 2013). Future studies designed to identify the regulatory pathways that favor one α-actinin isoform over the other would provide useful information into how tumor cells coordinate actin-binding proteins to facilitate complex processes such as macropinocytosis or metastasis.

The observation that α-actinin 4 is required for the uptake of N-PTX into tumor cells (Figure 5) points toward the cytoskeletal machinery in PDAC cells being able to regulate drug sensitivity via macropinocytosis. A historical problem in the treatment of cancer has been targeting the chemotherapeutic specifically to tumor cells and not healthy cells, and macropinocytosis represents a new mechanism by which this may be achieved, as the tumor cells are rapidly internalizing large amounts of extracellular material. Follow-up studies could be aimed at determining whether proteins like α-actinin 4, or other proteins that are required for macropinocytosis, could be utilized as predictive biomarkers of patient response to albumin- or nanoparticle-bound chemotherapeutics. Our studies also indicate that the α-actinin proteins localize to N-PTX–filled vesicles in PDAC cells (Figure 5); however, we do not know what the final fate of these vesicles is—whether they are retained within the cell or whether they are trafficked to a recycling compartment to remove the N-PTX from the tumor cells. Investigations into the vesicle trafficking machinery that acts downstream of macropinocytosis may provide insight into how to target tumor cells to block the efflux of chemotherapeutics after uptake and potentially improve the efficacy of these treatments for PDAC patients. There is a growing interest in drug design strategies focused on uptake by macropinocytosis, so understanding the cytoskeletal machinery that regulates the entry and trafficking of these drugs will give useful information into optimizing the design of these chemotherapies.

The observation that α-actinin 4 is required for collagen uptake into PDAC cells (Figure 2) and our previous work indicating a role for α-actinin 4 in the stabilization of invadopodia to remodel the ECM suggest that these two processes may be linked during metastatic dissemination of tumor cells. This presents new ideas about how cellular energy levels are maintained during metastasis, as macropinocytosis may provide a mechanism by which tumor cells can acquire nutrients regardless of whether they are in the primary tumor, in the vasculature, or at a secondary tissue. While the relationship between macropinocytosis and cell migration has not been well studied in tumor cells, there is a body of literature that states that these processes are antagonistic to one another in immune cells such as dendritic cells, which utilize macropinocytosis to take up antigen from the environment (Veltman, 2015; Bloomfield and Kay, 2016). It is possible that the requirement for actin and membranes is too high for cells to perform both processes simultaneously. In addition, molecular regulators may dictate the switch between macropinocytosis and migration. For example, myosin is localized to the rear of the dendritic cell during migration but moves to the front of the cell to perform macropinocytosis, thus halting cell motility (Chabaud *et al.*, 2015). Interesting recent evidence suggests that these processes may be cooperative, however, as it was recently demonstrated that macropinocytosis presents a mechanism by which dendritic cells can move against regions of high fluid pressure, allowing for dendritic cells to migrate to various regions of the body to sample antigens (Moreau *et al.*, 2019). This is potentially interesting in terms of PDAC, as the tumor is a region of high hydraulic pressure (Olive *et al.*, 2009; DuFort *et al.*, 2016; Weniger *et al.*, 2018), so macropinocytosis may represent a means by which tumor cells can break free of the tumor and begin to metastasize. While many of the chemical inhibitors of macropinocytosis, such as EIPA, also inhibit cell migration by disrupting actin dynamics, future studies designed at dissecting the two processes will be beneficial to understand whether macropinocytosis not only fuels tumor growth but also enhances the metastatic potential of PDAC cells.

In summary, our work here demonstrates an important role for the α-actinin proteins in the regulation of tumor cell growth via macropinocytosis, demonstrating that overexpression of actin-binding proteins in PDAC is able to enhance the proliferative rate of tumor cells in addition to the well-characterized role of cytoskeletal proteins during metastasis of tumor cells.

MATERIALS AND METHODS

Cell culture, antibodies, and reagents

MIA PaCa-2 and CFPAC-1 human pancreatic cancer cell lines were obtained from the American Type Culture Collection. Dan-G human pancreatic cancer cells were provided by Daniel Billadeau

FIGURE 5: Tumor cell growth is impacted by α-actinin 1 and 4, which enhance the uptake of nutrients and albumin-bound chemotherapeutics. (A, B) MTT assays were performed in MIA PaCa-2 cells after knockdown of α-actinin 1 (A) or α-actinin 4 (B). Cells were grown for 72 h in DMEM with low glutamine (0.2 mM) either with or without 3% BSA added. (C) MIA PaCa-2 cells were loaded with both TMR-dextran and Alexa 647–N-PTX. Arrows indicate colocalization between the two cargoes inside of vesicular compartments. (D, E) Alexa 647–N-PTX uptake assays were performed as described previously for TMR-dextran in MIA PaCa-2 cells, where knockdown of α-actinin 4 reduced uptake of Alexa 647–N-PTX. (F, G) Live cell imaging of MIA PaCa-2 cells expressing either GFP-α-actinin 1 (F) or GFP-α-actinin 4 (G) was performed after loading the cells for 20 min with Alexa 647–N-PTX. Boxed regions highlight areas where multiple GFP-α-actinin tails can be found associating with Alexa 647–N-PTX–filled vesicles. (H) Cartoon depicting the role of the α-actinin proteins in PDAC cell macropinocytosis. Cytoskeletal remodeling on the plasma membrane, which is required for invadopodia-based ECM cleavage and membrane ruffling during macropinocytosis, is dependent on actin cross-linking by α-actinin 4 to stabilize these structures and internalize multiple types of extracellular material, including albumin, collagen, and albuminized chemotherapeutics. After internalization, macropinosome trafficking is mediated by α-actinin 1 through the formation of actin comet tails, which propel vesicles through the cytoplasm. Depending on the cargo internalized via macropinocytosis, the α-actinin proteins can influence both tumor cell growth via trafficking of extracellular protein to the lysosome for degradation to provide nutrients, as well as susceptibility to the chemotherapeutic N-PTX that disrupts microtubule reorganization during cell division. Scale bars: 20 μm (C), 10 μm (D), 5 μm (F, G). Graphed data represent the mean ± SEM, and plotted data points represent average values for individual experiments, with at least three independent experiments performed. A total of 10 40× fields of cells were quantified for each condition per experiment for all macropinocytic uptake assays. Two-tailed Student's *t* test was used to measure statistical significance, and significant p values are shown above the graphs.

(Mayo Clinic). The 6741 human patient–derived xenograft (PDX) cells were isolated from pancreatic tumors implanted in nude mice as described previously (Sagar *et al.*, 2016) and were provided by the Mayo Clinic SPORE in Pancreatic Cancer. Tissues were collected from surgical resections for research purposes with written informed consent and were deidentified before use in research, and their use was approved by the Mayo Clinic Institutional Review Board (IRB). HPDE normal pancreas cells were obtained from Daniel Billadeau (Mayo Clinic). All cell lines were cultured in DMEM with 10% fetal bovine serum (FBS) and penicillin/streptomycin, except HPDE cells, which were maintained Keratinocyte-SFM with epidermal growth factor, bovine pituitary extract, and penicillin/streptomycin and regularly screened for mycoplasma by 4′,6-diamidino-2-phenylindole (DAPI) staining and PCR.

Antibodies used in this paper were α-actinin 1 (Santa-Cruz: sc1782 and Abcam: ab68194), α-actinin 4 (Abcam: ab108198), GAPDH (Cell Signaling: D16H11), Ki-67 (Cell Signaling: 12202), and p-ERK (Cell Signaling: 4377).

siRNA and expression construct transfection

Lipofectamine RNAiMax reagent (Invitrogen) was used according to the manufacturer's protocol for siRNA transfection in all PDAC cells lines. siRNA was used at 40–50 nM in Opti-MEM, and cells were cultured for 72 h in the presence of siRNA before being transferred to new dishes and experiments performed. The siRNA sequences used in this paper were nontargeting (Dharmacon: On-Target Plus #D-001810), human α-actinin 1 (Dharmacon: sense CACAGAUCGAGAACAUCGAAGUU), human α-actinin 4 #1 (Dharmacon: sense CCACAUCAGCUGGAAGGAUGGUCUU), and human α-actinin 4 #2 (Dharmacon: siGenome smartpool #M-011988-02).

Lipofectamine 3000 reagent (Invitrogen) was used according to the manufacturer's protocol for expression of fluorescently tagged constructs in PDAC cells. pEGFP-N1 α-actinin 1 was a gift from Carol Otey (UNC Chapel Hill, Addgene plasmid #11908), and human pEGFP-N1 α-actinin 4 was provided by Alan Wells at the University of Pittsburgh. LifeAct-mCherry and mEGFP-LifeAct-7 were provided by Michael Davidson (Florida State University, Addgene plasmid #54491, Addgene plasmid #54610). PM-mCherry was a gift from Elias T. Spiliotis at Drexel University. GFP-β-actin was provided by Gerard Marriott at the University of California, Berkeley.

SDS–PAGE and Western blotting to measure protein knockdown after siRNA transfection were performed as described previously (Burton *et al.*, 2020).

Macropinocytosis uptake assays

Seventy kilodalton TMR-dextran (ThermoFisher Scientific: #D1818) and TMR-BSA (ThermoFisher Scientific: #A23016) uptake assays were performed as described previously (Commisso *et al.*, 2014). Briefly, cells plated on collagen-coated coverslips were serum starved overnight, then pretreated with dimethyl sulfoxide (DMSO) or 70 μM EIPA (Millipore Sigma: #A3085) for 30 min, and inverted onto 50 μl drops of DMEM containing 1 mg/ml TMR-dextran or TMR-BSA for 20 min, followed by fixation and DAPI staining. The macropinocytic index ([area of dextran or BSA/total cell area] × 100) was calculated using ImageJ (Commisso *et al.*, 2014), and values were normalized to nontargeting siRNA control.

N-PTX (trade name: Abraxane) was purchased from the Mayo Clinic Pharmacy (Celgene: #103450). N-PTX was conjugated to the Alexa Fluor 647 far-red dye using the Protein Labeling Kit (Invitrogen: #A20173) according to the manufacturer's instructions. N-PTX uptake assays were performed as described above for TMR-dextran and TMR-BSA. N-PTX uptake was calculated as ([area of Alexa 647–N-PTX/total cell area] × 100), and values were set relative to nontargeting siRNA control.

DQ-collagen (ThermoFisher Scientific: #D12060) uptake assays were performed by plating cells on coverslips coated with 50 μg/ml type 1 rat tail collagen (Corning: #354236) and 25 μg/ml DQ-collagen for 16 h followed by fixation and DAPI staining. DQ-collagen uptake was calculated as ([area of DQ-collagen/total cell area] × 100), and values were set relative to nontargeting siRNA control.

Fluorescence microscopy

Following macropinocytosis uptake assays, cells plated on coverslips were prepared for immunofluorescence by being washed with Dulbecco's phosphate-buffered saline (D-PBS) followed by fixation (0.1 M PIPES, 1 mM ethylene glycol-bis(β-aminoethyl ether)-*N*,*N*,*N*′,*N*′-tetraacetic acid [EGTA], 3 mM $MgSO_4$, 2.5% paraformaldehyde, pH 7.0) at 37°C for 20 min. Coverslips were then washed in D-PBS, stained with DAPI, and mounted on glass slides using Prolong Gold (Thermo Fisher: P10144).

Live and fixed-cell imaging was performed on a Zeiss LSM 780 confocal microscope (Carl Zeiss, Oberkochen, Germany) controlled by Zeiss Zen Software (2012 SP1 black edition), as well as a Zeiss Axio Observer epifluorescence microscope. Images were acquired as single confocal slices through the same focal plane across all images in an experiment. Image processing was performed in Adobe Photoshop uniformly across the entire image. Cells were plated into 35 mm glass bottom imaging dishes (MatTek Corporation) before live cell imaging and maintained in a temperature-controlled environment (37°C, 5% CO_2). For live cell imaging of trafficking of TMR-dextran or Alexa 647–N-PTX, cells in imaging dishes were loaded for 20 min, followed by washing with Hank's Balanced Salt Solution (HBSS) and replacing the media for DMEM without labeled cargo, and then imaging was performed.

To determine the amount of α-actinin localized in the ruffling versus nonruffling areas of a cell, short time-lapse videos of 6741 cells expressing GFP-α-actinin 1 or 4 and PM-mCherry were acquired on a LSM780 confocal microscope. After the videos were acquired, 10-μm-long strips of the plasma membrane corresponding to ruffling and nonruffling areas were traced and the amounts of GFP-α-actinin and PM-mCherry were quantitated using the profile tool in Zen Black. The data were analyzed in Microsoft Excel, and the ratios of GFP-α-actinin:PM-mCherry in each region were determined. Ten cells over at least three experiments were quantitated for each actinin construct to determine the ratios. Analysis of macropinosome trafficking velocity and direction was performed using the TrackMate plug-in for ImageJ (Tinevez *et al.*, 2017).

Immunohistochemistry

Tissue microarray slides of paraffin-embedded human PDAC tumors as well as adjacent normal pancreas tissue were collected from patients during surgical resection, were deidentified, and were provided by the Mayo Clinic SPORE in Pancreatic Cancer. All patients provided written informed consent, and the study was approved by the Mayo Clinic IRB. Immunohistochemical staining was performed for each antibody as described previously (Burton *et al.*, 2020). Images were taken using a Zeiss Axio scope A1 microscope (Carl Zeiss, Thornwood, NY) configured for histological investigations. Images were captured with a Zeiss Axiocam 105 color digital camera driven by Zen 2 software (blue edition, 2011; Carl Zeiss Microscopy, GmbH).

FRAP

MIA PaCa-2 cells expressing GFP-β-actin after knockdown of the indicated proteins were imaged on a Zeiss LSM 780 confocal

microscope in 35 mm glass bottom imaging dishes. Cells were imaged at a rate of one frame per 2 s for five frames to measure baseline fluorescence, and then a boxed region of the plasma membrane was photobleached and imaging was continued for 50 s to measure the FRAP. The mean fluorescence intensity of the photobleached region was calculated using ImageJ, and values were first normalized to the average of the prebleach values and then normalized so the frame after the bleach was set to 0. The percent FRAP was calculated as the average percentage of actin fluorescence recovery after 50 s postbleach, and the half-time of recovery was calculated using a nonlinear regression curve analysis from GraphPad Prism.

Rhodamine actin incorporation assay

Following knockdown of α-actinin 1 or α-actinin 4, MIA PaCa-2 cells were seeded onto poly-L-lysine (Sigma: #P8920)-coated coverslips and serum starved with serum-free media for 3 h before actin incorporation. Rhodamine-labeled actin (Cytoskeleton: #AR05) was prepared by diluting to 12 μM with G-actin buffer (5 mM Tris-HCl, 0.2 mM $CaCl_2$, 0.2 mM ATP, 1 mM dithiothreitol, pH 8.0). Cells were permeabilized for 15 min with buffer C (138 mM KCl, 10 mM PIPES, 0.1 mM ATP, 3 mM EGTA, 4 mM $MgCl_2$, 1% BSA, 0.025% saponin, pH 6.9) containing 1 μM rhodamine-labeled actin at room temperature, followed by fixation and then gentle washing with PBS. The cells were stained with phalloidin FITC (Sigma: #P5282) used at a concentration of 1:300 in blocking buffer (5% goat serum, 5% glycerol, 0.2% NaN_3, pH 7.2, in D-PBS) for 1 h at 37°C, followed by staining with Hoechst (Invitrogen: #H3570). Actin incorporation was analyzed using ImageJ to measure the mean pixel density of rhodamine actin present in the cells.

DQ-BSA macropinosome trafficking assay

For DQ-BSA trafficking experiments (Figure 4, H–J; Supplemental Figure 3, C–G), cells were treated the same as for uptake assays and then loaded with 1 mg/ml TMR-dextran and 0.5 mg/ml DQ Green BSA (ThermoFisher: D12050) for 20 min by inverting coverslips onto 50 μl drops of DMEM containing the two macropinocytic cargoes. Cells were washed with HBSS, and then chased in DMEM without dextran or DQ-BSA for 0–120 min. The macropinocytic index for TMR-dextran was calculated as described above. DQ-BSA trafficking efficiency was calculated as (area of DQ-BSA/total cell area) × 100, and values were set relative to the nontargeting siRNA 120 min chase condition, representing the maximal amount of DQ-BSA fluorescence in the lysosome.

For the Lysotracker trafficking experiments (Figure 4, F and G; Supplemental Figure 3, F and G), following the 72 h knockdown of α-actinin 1 or nontargeting control, MIA-PaCa2 cells were labeled with Lysotracker Blue (Invitrogen: #L7525) for 1 h, washed with DMEM, and then loaded with 1 mg/ml TMR-dextran and 0.5 mg/ml DQ Green BSA as described above. Cells were then washed with HBSS and chased in DMEM for 0 or 120 min. Images were collected in live cells at 0 or 120 min on a Zeiss LSM780 confocal microscope. The number of dextran vesicles colocalized with lysosomes labeled with Lysotracker Blue was divided by the total number of dextran vesicles to determine the total percentage of dextran and Lysotracker colocalization. The same images were also used to count the DQ-BSA vesicles colocalized with Lysotracker Blue.

Lysosome number quantification

Lysosome number was quantified by labeling cells with Lysotracker Deep Red (Invitrogen: #L12492) for 1 h and then collecting images in live cells on a Zeiss LSM780 confocal microscope. The lysosome number per cell was quantified using ImageJ.

Cell viability assays

Cell viability was measured using the CellTiter 96 Non-Radioactive Cell Proliferation Assay (Promega: G4000) according to the manufacturer's instructions. For the cell viability assays in Figure 1, MIA PaCa-2 (3000 cells/well) and Dan-G (6000 cells/well) cells were plated in 96-well plates after a 72 h siRNA knockdown of the indicated proteins in DMEM + 10% FBS and pen/strep. Cell viability was measured 24, 72, and 120 h postplating in triplicate for each condition; absorbance values were set relative to nontargeting siRNA control. For the cell viability assays in Figure 5, MIA Paca-2 cells were plated in 96-well plates in DMEM + 10% FBS and pen/strep after a 72 h knockdown of the indicated proteins. The following day, the media was replaced with DMEM without glutamine (ThermoFisher: 21068-028) and supplemented with L-glutamine to a final concentration of 0.2 mM (low glutamine) either with or without 3% BSA (Millipore Sigma: 126609) as indicated. The media was replaced every 24 h, and cell viability measurements were taken after 72 h in triplicate for each condition.

Statistical analysis

Microsoft Excel was used to perform two-tailed Student's *t* test analysis between two groups for each experiment, and graphs were made using GraphPad Prism. Graphed data represent the mean ± SEM, and significant *p* values are shown above the graphs, while nonsignificant *p* values are indicated by N.S.

ACKNOWLEDGMENTS

This research was funded by Grant R01 CA104125 from the National Cancer Institute (M.A.M., G.L.R.), the Mayo Clinic Center for Cell Signaling in Gastroenterology (P30 DK084567), the Mayo Clinic SPORE in Pancreatic Cancer (P50 CA102701), the Mayo Clinic Center for Biomedical Discovery, the Mayo Clinic Cancer Center, and the Mayo Clinic Graduate School of Biomedical Sciences (K.M.B.).

REFERENCES

Al-Batran SE, Geissler M, Seufferlein T, Oettle H (2014). Nab-paclitaxel for metastatic pancreatic cancer: clinical outcomes and potential mechanisms of action. Oncol Res Treat 37, 128–134.

An HT, Yoo S, Ko J (2016). α-Actinin-4 induces the epithelial-to-mesenchymal transition and tumorigenesis via regulation of Snail expression and beta-catenin stabilization in cervical cancer. Oncogene 35, 5893–5904.

Araki N, Hatae T, Yamada T, Hirohashi S (2000). Actinin-4 is preferentially involved in circular ruffling and macropinocytosis in mouse macrophages: analysis by fluorescence ratio imaging. J Cell Sci 113 (Pt 18), 3329–3340.

Babakov VN, Petukhova OA, Turoverova LV, Kropacheva IV, Tentler DG, Bolshakova AV, Podolskaya EP, Magnusson KE, Pinaev GP (2008). RelA/NF-kappaB transcription factor associates with alpha-actinin-4. Exp Cell Res 314, 1030–1038.

Bloomfield G, Kay RR (2016). Uses and abuses of macropinocytosis. J Cell Sci 129, 2697–2705.

Bryant KL, Mancias JD, Kimmelman AC, Der CJ (2014). KRAS: feeding pancreatic cancer proliferation. Trends Biochem Sci 39, 91–100.

Buckley CM, Pots H, Gueho A, Vines JH, Munn CJ, Phillips BA, Gilsbach B, Traynor D, Nikolaev A, Soldati T, *et al.* (2020). Coordinated Ras and Rac activity shapes macropinocytic cups and enables phagocytosis of geometrically diverse bacteria. Curr Biol 30, 2912–2926.

Burton KM, Cao H, Chen J, Qiang L, Krueger EW, Johnson KM, Bamlet WR, Zhang L, McNiven MA, Razidlo GL (2020). Dynamin 2 interacts with alpha-actinin 4 to drive tumor cell invasion. Mol Biol Cell 31, 439–451.

Buscail L, Bournet B, Cordelier P (2020). Role of oncogenic KRAS in the diagnosis, prognosis and treatment of pancreatic cancer. Nat Rev Gastroenterol Hepatol 17, 153–168.

Chabaud M, Heuze ML, Bretou M, Vargas P, Maiuri P, Solanes P, Maurin M, Terriac E, Le Berre M, Lankar D, *et al.* (2015). Cell migration and antigen

capture are antagonistic processes coupled by myosin II in dendritic cells. Nat Commun 6, 7526.
Chan AY, Bailly M, Zebda N, Segall JE, Condeelis JS (2000). Role of cofilin in epidermal growth factor-stimulated actin polymerization and lamellipod protrusion. J Cell Biol 148, 531–542.
Chan AY, Raft S, Bailly M, Wyckoff JB, Segall JE, Condeelis JS (1998). EGF stimulates an increase in actin nucleation and filament number at the leading edge of the lamellipod in mammary adenocarcinoma cells. J Cell Sci 111 (Pt 2), 199–211.
Commisso C, Davidson SM, Soydaner-Azeloglu RG, Parker SJ, Kamphorst JJ, Hackett S, Grabocka E, Nofal M, Drebin JA, Thompson CB, *et al.* (2013). Macropinocytosis of protein is an amino acid supply route in Ras-transformed cells. Nature 497, 633–637.
Commisso C, Flinn RJ, Bar-Sagi D (2014). Determining the macropinocytic index of cells through a quantitative image-based assay. Nat Protoc 9, 182–192.
Corbett-Nelson EF, Mason D, Marshall JG, Collette Y, Grinstein S (2006). Signaling-dependent immobilization of acylated proteins in the inner monolayer of the plasma membrane. J Cell Biol 174, 255–265.
Cullis J, Siolas D, Avanzi A, Barui S, Maitra A, Bar-Sagi D (2017). Macropinocytosis of Nab-paclitaxel drives macrophage activation in pancreatic cancer. Cancer Immunol Res 5, 182–190.
Dolat L, Spiliotis ET (2016). Septins promote macropinosome maturation and traffic to the lysosome by facilitating membrane fusion. J Cell Biol 214, 517–527.
DuFort CC, DelGiorno KE, Carlson MA, Osgood RJ, Zhao C, Huang Z, Thompson CB, Connor RJ, Thanos CD, Scott Brockenbrough J, *et al.* (2016). Interstitial pressure in pancreatic ductal adenocarcinoma is dominated by a gel-fluid phase. Biophys J 110, 2106–2119.
Elia I, Doglioni G, Fendt SM (2018). Metabolic hallmarks of metastasis formation. Trends Cell Biol 28, 673–684.
Fehrenbacher K, Huckaba T, Yang HC, Boldogh I, Pon L (2003). Actin comet tails, endosomes and endosymbionts. J Exp Biol 206, 1977–1984.
Foley KS, Young PW (2013). An analysis of splicing, actin-binding properties, heterodimerization and molecular interactions of the non-muscle alpha-actinins. Biochem J 452, 477–488.
Foley KS, Young PW (2014). The non-muscle functions of actinins: an update. Biochem J 459, 1–13.
Fujii M, Kawai K, Egami Y, Araki N (2013). Dissecting the roles of Rac1 activation and deactivation in macropinocytosis using microscopic photo-manipulation. Sci Rep 3, 2385.
Fukumoto M, Kurisu S, Yamada T, Takenawa T (2015). α-Actinin-4 enhances colorectal cancer cell invasion by suppressing focal adhesion maturation. PLoS One 10, e0120616.
Ha KD, Bidlingmaier SM, Liu B (2016). Macropinocytosis exploitation by cancers and cancer therapeutics. Front Physiol 7, 381.
Honda K (2015). The biological role of actinin-4 (ACTN4) in malignant phenotypes of cancer. Cell Biosci 5, 41.
Honda K, Yamada T, Hayashida Y, Idogawa M, Sato S, Hasegawa F, Ino Y, Ono M, Hirohashi S (2005). Actinin-4 increases cell motility and promotes lymph node metastasis of colorectal cancer. Gastroenterology 128, 51–62.
Hosseini K, Sbosny L, Poser I, Fischer-Friedrich E (2020). Binding dynamics of α-actinin-4 in dependence of actin cortex tension. Biophys J 119, 1091–1107.
Izaguirre G, Aguirre L, Hu YP, Lee HY, Schlaepfer DD, Aneskievich BJ, Haimovich B (2001). The cytoskeletal/non-muscle isoform of alpha-actinin is phosphorylated on its actin-binding domain by the focal adhesion kinase. J Biol Chem 276, 28676–28685.
Kamerkar S, LeBleu VS, Sugimoto H, Yang S, Ruivo CF, Melo SA, Lee JJ, Kalluri R (2017). Exosomes facilitate therapeutic targeting of oncogenic KRAS in pancreatic cancer. Nature 546, 498–503.
Kamphorst JJ, Nofal M, Commisso C, Hackett SR, Lu W, Grabocka E, Vander Heiden MG, Miller G, Drebin JA, Bar-Sagi D, *et al.* (2015). Human pancreatic cancer tumors are nutrient poor and tumor cells actively scavenge extracellular protein. Cancer Res 75, 544–553.
Kikuchi S, Honda K, Tsuda H, Hiraoka N, Imoto I, Kosuge T, Umaki T, Onozato K, Shitashige M, Yamaguchi U, *et al.* (2008). Expression and gene amplification of actinin-4 in invasive ductal carcinoma of the pancreas. Clin Cancer Res 14, 5348–5356.
Kim SM, Nguyen TT, Ravi A, Kubiniok P, Finicle BT, Jayashankar V, Malacrida L, Hou J, Robertson J, Gao D, *et al.* (2018). PTEN deficiency and AMPK activation promote nutrient scavenging and anabolism in prostate cancer cells. Cancer Discov 8, 866–883.
Koivusalo M, Welch C, Hayashi H, Scott CC, Kim M, Alexander T, Touret N, Hahn KM, Grinstein S (2010). Amiloride inhibits macropinocytosis by lowering submembranous pH and preventing Rac1 and Cdc42 signaling. J Cell Biol 188, 547–563.
Kovac B, Makela TP, Vallenius T (2018). Increased α-actinin-1 destabilizes E-cadherin-based adhesions and associates with poor prognosis in basal-like breast cancer. PLoS One 13, e0196986.
Labuschagne CF, Cheung EC, Blagih J, Domart MC, Vousden KH (2019). Cell clustering promotes a metabolic switch that supports metastatic colonization. Cell Metab 30, 720–734.e725.
Liu H, Sun M, Liu Z, Kong C, Kong W, Ye J, Gong J, Huang DCS, Qian F (2019). KRAS-enhanced macropinocytosis and reduced FcRn-mediated recycling sensitize pancreatic cancer to albumin-conjugated drugs. J Control Release 296, 40–53.
Liu X, Ghosh D (2019). Intracellular nanoparticle delivery by oncogenic KRAS-mediated macropinocytosis. Int J Nanomedicine 14, 6589–6600.
Meyer RK, Aebi U (1990). Bundling of actin filaments by alpha-actinin depends on its molecular length. J Cell Biol 110, 2013–2024.
Moreau HD, Blanch-Mercader C, Attia R, Maurin M, Alraies Z, Sanseau D, Malbec O, Delgado MG, Bousso P, Joanny JF, *et al.* (2019). Macropinocytosis overcomes directional bias in dendritic cells due to hydraulic resistance and facilitates space exploration. Dev Cell 49, 171–188.e175.
Morita R, Nakano K, Shigeta Y, Harada R (2020). Molecular mechanism for the actin-binding domain of α-actinin Ain1 elucidated by molecular dynamics simulations and mutagenesis experiments. J Phys Chem B 124, 8495–8503.
Mukhina S, Wang YL, Murata-Hori M (2007). Alpha-actinin is required for tightly regulated remodeling of the actin cortical network during cytokinesis. Dev Cell 13, 554–565.
Murphy ACH, Young PW (2015). The actinin family of actin cross-linking proteins—a genetic perspective. Cell Biosci 5, 49.
Olivares O, Mayers JR, Gouirand V, Torrence ME, Gicquel T, Borge L, Lac S, Roques J, Lavaut MN, Berthezene P, *et al.* (2017). Collagen-derived proline promotes pancreatic ductal adenocarcinoma cell survival under nutrient limited conditions. Nat Commun 8, 16031.
Olive KP, Jacobetz MA, Davidson CJ, Gopinathan A, McIntyre D, Honess D, Madhu B, Goldgraben MA, Caldwell ME, Allard D, *et al.* (2009). Inhibition of Hedgehog signaling enhances delivery of chemotherapy in a mouse model of pancreatic cancer. Science 324, 1457–1461.
Orth JD, Krueger EW, Cao H, McNiven MA (2002). The large GTPase dynamin regulates actin comet formation and movement in living cells. Proc Natl Acad Sci USA 99, 167–172.
Orth M, Metzger P, Gerum S, Mayerle J, Schneider G, Belka C, Schnurr M, Lauber K (2019). Pancreatic ductal adenocarcinoma: biological hallmarks, current status, and future perspectives of combined modality treatment approaches. Radiat Oncol 14, 141.
Papalazarou V, Zhang T, Paul NR, Juin A, Cantini M, Maddocks ODK, Salmeron-Sanchez M, Machesky LM (2020). The creatine-phosphagen system is mechanoresponsive in pancreatic adenocarcinoma and fuels invasion and metastasis. Nat Metab 2, 62–80.
Pizarro-Cerda J, Chorev DS, Geiger B, Cossart P (2017). The diverse family of Arp2/3 complexes. Trends Cell Biol 27, 93–100.
Qian Y, Wang X, Liu Y, Li Y, Colvin RA, Tong L, Wu S, Chen X (2014). Extracellular ATP is internalized by macropinocytosis and induces intracellular ATP increase and drug resistance in cancer cells. Cancer Lett 351, 242–251.
Quick Q, Skalli O (2010). Alpha-actinin 1 and alpha-actinin 4: contrasting roles in the survival, motility, and RhoA signaling of astrocytoma cells. Exp Cell Res 316, 1137–1147.
Rajeshkumar NV, Yabuuchi S, Pai SG, Tong Z, Hou S, Bateman S, Pierce DW, Heise C, Von Hoff DD, Maitra A, Hidalgo M (2016). Superior therapeutic efficacy of nab-paclitaxel over cremophor-based paclitaxel in locally advanced and metastatic models of human pancreatic cancer. Br J Cancer 115, 442–453.
Ramirez C, Hauser AD, Vucic EA, Bar-Sagi D (2019). Plasma membrane V-ATPase controls oncogenic RAS-induced macropinocytosis. Nature 576, 477–481.
Roy I, McAllister DM, Gorse E, Dixon K, Piper CT, Zimmerman NP, Getschman AE, Tsai S, Engle DD, Evans DB, *et al.* (2015). Pancreatic cancer cell migration and metastasis is regulated by chemokine-biased agonism and bioenergetic signaling. Cancer Res 75, 3529–3542.
Sagar G, Sah RP, Javeed N, Dutta SK, Smyrk TC, Lau JS, Giorgadze N, Tchkonia T, Kirkland JL, Chari ST, Mukhopadhyay D (2016). Pathogenesis of pancreatic cancer exosome-induced lipolysis in adipose tissue. Gut 65, 1165–1174.
Shao H, Li S, Watkins SC, Wells A (2014). α-Actinin-4 is required for amoeboid-type invasiveness of melanoma cells. J Biol Chem 289, 32717–32728.

Shao H, Wu C, Wells A (2010). Phosphorylation of alpha-actinin 4 upon epidermal growth factor exposure regulates its interaction with actin. J Biol Chem 285, 2591–2600.
Siegel RL, Miller KD, Jemal A (2018). Cancer statistics, 2018. CA Cancer J Clin 68, 7–30.
Sjoblom B, Salmazo A, Djinovic-Carugo K (2008). Alpha-actinin structure and regulation. Cell Mol Life Sci 65, 2688–2701.
Surcel A, Schiffhauer ES, Thomas DG, Zhu Q, DiNapoli KT, Herbig M, Otto O, West-Foyle H, Jacobi A, Krater M, *et al.* (2019). Targeting mechanoresponsive proteins in pancreatic cancer: 4-hydroxyacetophenone blocks dissemination and invasion by activating MYH14. Cancer Res 79, 4665–4678.
Swanson JA (2008). Shaping cups into phagosomes and macropinosomes. Nat Rev Mol Cell Biol 9, 639–649.
Tang VW, Brieher WM (2012). α-Actinin-4/FSGS1 is required for Arp2/3-dependent actin assembly at the adherens junction. J Cell Biol 196, 115–130.
Tinevez JY, Perry N, Schindelin J, Hoopes GM, Reynolds GD, Laplantine E, Bednarek SY, Shorte SL, Eliceiri KW (2017). TrackMate: an open and extensible platform for single-particle tracking. Methods 115, 80–90.
Veltman DM (2015). Drink or drive: competition between macropinocytosis and cell migration. Biochem Soc Trans 43, 129–132.
Von Hoff DD, Ervin T, Arena FP, Chiorean EG, Infante J, Moore M, Seay T, Tjulandin SA, Ma WW, Saleh MN, *et al.* (2013). Increased survival in pancreatic cancer with nab-paclitaxel plus gemcitabine. N Engl J Med 369, 1691–1703.
Wang MC, Chang YH, Wu CC, Tyan YC, Chang HC, Goan YG, Lai WW, Cheng PN, Liao PC (2015). Alpha-actinin 4 is associated with cancer cell motility and is a potential biomarker in non-small cell lung cancer. J Thorac Oncol 10, 286–301.
Waters AM, Der CJ (2018). KRAS: the critical driver and therapeutic target for pancreatic cancer. Cold Spring Harb Perspect Med 8, a031435.
Welsch T, Keleg S, Bergmann F, Bauer S, Hinz U, Schmidt J (2009). Actinin-4 expression in primary and metastasized pancreatic ductal adenocarcinoma. Pancreas 38, 968–976.
Weniger M, Honselmann KC, Liss AS (2018). The extracellular matrix and pancreatic cancer: a complex relationship. Cancers (Basel) 10, 316.
Xie GF, Zhao LD, Chen Q, Tang DX, Chen QY, Lu HF, Cai JR, Chen Z (2020). High ACTN1 is associated with poor prognosis, and ACTN1 silencing suppresses cell proliferation and metastasis in oral squamous cell carcinoma. Drug Des Devel Ther 14, 1717–1727.
Xu J, Wirtz D, Pollard TD (1998). Dynamic cross-linking by alpha-actinin determines the mechanical properties of actin filament networks. J Biol Chem 273, 9570–9576.
Yamaguchi H, Ito Y, Miura N, Nagamura Y, Nakabo A, Fukami K, Honda K, Sakai R (2017). Actinin-1 and actinin-4 play essential but distinct roles in invadopodia formation by carcinoma cells. Eur J Cell Biol 96, 685–694.
Yamamoto S, Tsuda H, Honda K, Kita T, Takano M, Tamai S, Inazawa J, Yamada T, Matsubara O (2007). Actinin-4 expression in ovarian cancer: a novel prognostic indicator independent of clinical stage and histological type. Mod Pathol 20, 1278–1285.
Yang X, Pang Y, Zhang J, Shi J, Zhang X, Zhang G, Yang S, Wang J, Hu K, Wang J, *et al.* (2019). High expression levels of ACTN1 and ACTN3 indicate unfavorable prognosis in acute myeloid leukemia. J Cancer 10, 4286–4292.
Ying H, Kimmelman AC, Lyssiotis CA, Hua S, Chu GC, Fletcher-Sananikone E, Locasale JW, Son J, Zhang H, Coloff JL, *et al.* (2012). Oncogenic Kras maintains pancreatic tumors through regulation of anabolic glucose metabolism. Cell 149, 656–670.
Zhao H, Yang L, Baddour J, Achreja A, Bernard V, Moss T, Marini JC, Tudawe T, Seviour EG, San Lucas FA, *et al.* (2016). Tumor microenvironment derived exosomes pleiotropically modulate cancer cell metabolism. eLife 5, e10250.